

## REVIEW

# Diffusion-weighted imaging of the liver: an update

N. Bharwani<sup>a</sup>, D.M. Koh<sup>b</sup>

<sup>a</sup>Department of Radiology, St Mary's Hospital, Imperial College Healthcare NHS Trust, London, UK; <sup>b</sup>Department of Radiology, Royal Marsden Hospital, Sutton, UK

Corresponding address: Dr Nishat Bharwani, Consultant Radiologist, Department of Radiology, St Mary's Hospital, Imperial College Healthcare NHS Trust, 3rd Floor Queen Elizabeth The Queen Mother Building, Praed Street, London W2 1NY, UK.

Email: nishat.bharwani@imperial.nhs.uk

Date accepted for publication 25 February 2013

### Abstract

Diffusion-weighted magnetic resonance imaging (DW-MRI) is now widely used as a standard imaging sequence for evaluation of the liver. The technique is easy to implement across different MRI platforms, and results in enhanced disease detection and characterization. With careful implementation, the quantitative apparent diffusion coefficient derived shows good measurement reproducibility, which can be applied for tissue characterization, the assessment of tumour response and disease prognostication. There is now a body of evidence that highlights the relative strengths and limitations of the technique for the assessment of liver diseases. The potential for more sophisticated analysis of DW-MRI data is currently being widely investigated.

**Keywords:** *Diffusion-weighted magnetic resonance imaging; liver.*

## Background

Magnetic resonance imaging (MRI) is playing an increasing role in the assessment of patients with liver disease due to its high soft tissue resolution, lack of ionizing radiation and ability to provide functional data. Diffusion-weighted (DW)-MRI is a functional imaging technique that is now widely used as a standard imaging sequence, together with unenhanced T1/T2 weighted imaging and contrast-enhanced imaging for liver evaluation.

As a non-contrast-enhanced technique, DW-MRI is particularly useful in patients with severe renal dysfunction at risk of developing nephrogenic systemic fibrosis (NSF) after administration of gadolinium-based contrast medium<sup>[1–4]</sup>. The clinical uses of liver DW-MRI include improved detection of focal liver lesions, contribution to tissue characterization for both diffuse disease and focal lesions, monitoring of tumour response after chemotherapy or radiotherapy, detection of recurrent disease, differentiating recurrence from post-therapeutic change, and potentially predicting treatment outcome. Knowledge of the evidence highlighting the strengths and limitations of the technique in these areas is important to maximize the

advantages of using DW-MRI and to avoid the potential pitfalls.

## General principles of liver DW-MRI

DW-MRI is a technique that explores the random, thermally driven, motion of water protons in the body, deriving image contrast on the basis of differences in water diffusivity within tissues. Water protons in the body exist in the intra- and extracellular spaces; free diffusion is modified by bulk capillary flow and the interactions of the protons with cell membranes and macromolecules. In this way, DW-MRI provides an insight into cellular architecture at the micrometre scale. In highly cellular tissues (e.g. tumour tissue), the tortuosity of the extracellular space and cell membrane density limit the apparent diffusion of water, which is said to be impeded<sup>[5,6]</sup>. In contrast, cystic and necrotic tissues have fewer barriers to water diffusion and the apparent diffusion is relatively free.

The sensitivity of DW-MRI to water diffusion is altered by changing the *b* value of the sequence, a parameter that is proportional to the gradient amplitude, duration of the

**Table 1** Typical MRI parameters for performing free-breathing DWI liver imaging at 1.5 T and 3.0 T

	Imaging at 3.0 T	Imaging at 1.5 T
Field of view (cm)	380–400	380–400
Matrix size	112 × 256	112 × 256
Repetition time (ms)	3300	4500
Echo time (ms)	72	72
Echo-planar imaging factor	84	104
Parallel imaging factor	2	2
No. of signals averaged	3	6
Receiver bandwidth (Hz pixel <sup>-1</sup> )	2056	1760
Section thickness (mm)	5	5
Direction of motion probing gradients	Phase, frequency and slice (3 scan trace)	Phase, frequency and slice (3 scan trace)
Fat suppression	SPAIR	SPAIR
<i>b</i> factors (s mm <sup>-2</sup> )	0, 100, 500, 750	Multiple <i>b</i> values: 0, 100, 500, 750

SPAIR, spectral-attenuated inversion recovery.

applied gradient and time interval between the 2 gradients. Protons with larger diffusion distances, e.g. in the intravascular space, show steep signal attenuation at low *b* values ( $b < 100\text{--}150\text{ s mm}^{-2}$ ). By contrast, cellular tissues (e.g. tumours) with more impeded water diffusion tend to maintain their signal at higher *b* values ( $>500\text{ s mm}^{-2}$ ). Therefore, increasing *b* values result in greater signal attenuation in less cellular areas, e.g. normal liver parenchyma, compared with cellular areas, e.g. tumours, in this way improving and maximizing the contrast between cellular disease and the background liver parenchyma. Visual assessment in this way also enables qualitative disease evaluation based on differential signal attenuation between tissues with increasing diffusion weighting.

The data obtained from 2 or more (typically 3) *b* values<sup>[7]</sup> is used to generate the apparent diffusion coefficient (ADC) maps. To achieve this, the signal intensity (or logarithm of the signal intensity) from each image voxel measured at increasing *b* values is plotted against the *b* value to generate a graph, and the slope of this line is the ADC for that single voxel. The mathematical equation used to calculate the ADC is  $ADC = \ln(SI_0/SI)/b$ , where  $SI_0$  is the signal intensity for  $b=0$  and  $SI$  is the signal intensity for a higher *b* value. On the MR scanner, this process is automated for all voxels and a parametric ADC map is produced.

## Technical considerations

With growing equalization of technology across MR vendor platforms, there is now a significant convergence in the implementation of DW-MRI across different scanners. The most widely used technique is fat-suppressed single-shot spin-echo echo-planar imaging, which can be performed in breathhold, free-breathing or with respiratory triggering. In the clinical setting, the free-breathing technique is now most frequently used, as multiple signal averaging improves the image signal-to-noise ratio (SNR) especially at higher *b* values. However, a detailed discussion of the technical implementation of liver DW-MRI is

beyond the scope of this article. The reader is referred to previously published papers on the subject<sup>[8–14]</sup>.

A typical diffusion-weighted MR imaging protocol at 1.5 T and 3.0 T is listed in Table 1. In general, the quality of liver DW-MRI seems to be more consistent at 1.5 T compared with 3.0 T, although many institutions are now adopting the 3.0 T imaging platform for liver imaging because of the high-quality T1-weighted dynamic contrast-enhanced imaging that can be achieved at the higher field strength.

## DW image interpretation

Visual assessment of DW-MR images is useful in disease detection and lesion characterization based on differential signal attenuation within tissues. Cellular tissues demonstrate impeded diffusion, which shows high signal intensity at higher *b* values and a corresponding low ADC value. Cystic or necrotic tissues show greater signal attenuation on higher *b* values and return higher ADC values. However, the signal return on diffusion images is related to both the proton diffusivity within a tissue and the T2 relaxation time of that tissue. Therefore lesions may appear to show impeded diffusion on the high *b* value images (i.e. returning high signal intensity) as a result of their intrinsic long T2 relaxation time rather than impeded water diffusivity. This phenomenon is known as T2 shine-through and may be encountered in hepatic cysts and liver haemangiomas. It is recognized by correlating the high *b* value images with the ADC map; regions with T2 shine-through also return high ADC values.

Quantification of tissue diffusivity is performed using ADC maps, which can be evaluated visually or by drawing regions of interest on the ADC map to generate mean ADC values for the tissue/region of interest. These quantitative measures are being used to characterize both focal and diffuse liver pathology and in the prediction and assessment of tumour response to treatment. However, to enable meaningful interpretation and for confidence in ascribing an observed ADC change to real treatment effects rather than to biological,

instrumental or observer variations, it is important to establish the ADC measurement reproducibility of the scanner system<sup>[15–18]</sup>. Unfortunately, as each scanner and the conditions of measurements are different, reproducibility measurements should be verified on individual scanners and could be built into the departmental quality assurance programme, which includes the use of dedicated diffusion phantoms<sup>[19]</sup>.

The measurement reproducibility of a scanner can be established using a small cohort of patients (typically about 10–12) who are scanned twice on the same scanner using the same imaging parameters on different days or times. By performing Bland–Altman statistical analysis on the mean ADC result obtained on each measurement in each patient, we can calculate the coefficient of repeatability ( $R$ ). This provides the 95% confidence limits of the ADC measurement variation on a per patient basis. For example, a coefficient of repeatability of 13% suggests that by using the particular DW-MRI technique, a change in the ADC value of more than 13% is unlikely to be due to chance. Measurement reproducibility calculated from normal tissues may not be applicable to the disease as disease processes (e.g. tumours) are often heterogeneous and thus result in poorer measurement reproducibility compared with normal tissues<sup>[20]</sup>.

Nevertheless, free-breathing DW-MRI has been found to provide the most reproducible ADC results compared with breathhold or respiratory-triggered DW-MRI<sup>[15]</sup>. Furthermore, by meticulous technique, it is possible to achieve measurement reproducibility of less than 10% using free-breathing DW-MRI. In the reported literature, a coefficient of repeatability of 20–40% is typical<sup>[15,18,21,22]</sup>.

## Clinical applications of liver DW-MRI: diffuse diseases

### *Fibrosis/cirrhosis*

Liver fibrosis resulting from alcoholic or infective hepatitis is an important cause of morbidity and mortality. As clinical examination and biochemical markers are unreliable for staging hepatic fibrosis, the gold standard for establishing liver fibrosis is by histologic evaluation after liver biopsy. However, this is invasive and prone to sampling errors<sup>[23,24]</sup>, intra-observer variation<sup>[25]</sup> and potential complications<sup>[26]</sup>. Hence, there is desire for a reliable, non-invasive means of assessing disease severity in patients with chronic liver disease. Although conventional computed tomography (CT) and MRI can identify patients with advanced liver cirrhosis, the evaluation of early hepatic fibrosis and inflammation is impossible with conventional MRI, and newer sequences such as DW-MRI and MR elastography are currently under evaluation.

Several studies have shown that the cirrhotic liver is associated with lower ADC values than normal liver

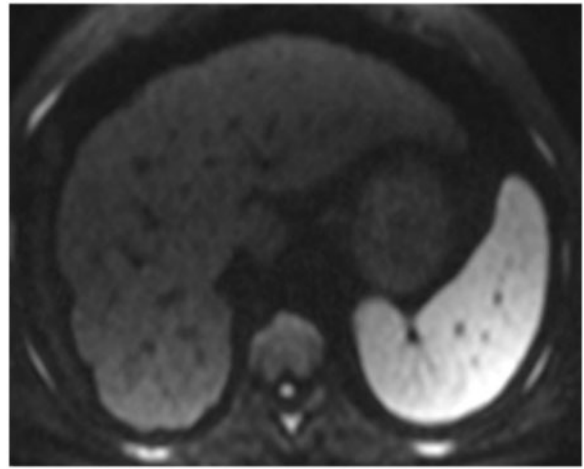


**Figure 1** A 46-year-old with liver cirrhosis. The  $b = 750 \text{ s mm}^{-2}$  image shows an irregular liver outline, which also returns higher signal intensity compared with normal liver due to impeded water diffusion.

parenchyma (Fig. 1)<sup>[27–31]</sup> and higher grades of cirrhosis are associated with lower ADC values<sup>[29,32]</sup> (Table 2). The reduction in water diffusivity seen with hepatic fibrosis is likely to be multifactorial but has in part been attributed to the increase in collagen within the liver, which has a lower unbound water content than normal hepatic parenchyma<sup>[33,34]</sup>. In 2 studies, decrease in hepatic perfusion was cited as a reason because decreased liver perfusion fraction was observed in the cirrhotic liver, measured using multiple  $b$  value DW-MRI and analysed using the principles of intravoxel incoherent motion (IVIM)<sup>[35,36]</sup>.

A recent retrospective study by Fujimoto et al.<sup>[37]</sup> assessed hepatic entropy ADC values in addition to mean ADC values in patients with chronic hepatitis C. The entropy ADC provides information related to variation in the volume histogram of ADC and has previously been applied in the neurologic system<sup>[38,39]</sup>. A wider distribution in histogram values leads to a larger entropy ADC value. As in previous studies, the authors showed that the mean hepatic ADC decreased with increasing grades of fibrosis/inflammation. In addition, entropy ADC was shown to increase with fibrosis, which correlated strongly with fibrosis score and inflammatory activity grade.

Table 2 summarizes published papers utilizing DW-MRI for the assessment of liver fibrosis. From these studies, the mean ADC values measured on DW-MRI seem to have a limited range to distinguish early stages of fibrosis (e.g. METAVAR grades I and II, where medical intervention may be possible) from more advanced disease, thus limiting the use of the technique in this disease context. In one study comparing MR elastography with DW-MRI, MR elastography was more sensitive than DW-MRI in diagnosing early stages of liver fibrosis. With technologic advancement, it may be possible to

**Table 2** Selected publications on the use of DWI for the assessment of liver cirrhosis.

Study	No of patients	Key findings
Do et al. <sup>[77]</sup>	56	Normalized liver ADC relative to spleen improved measurement reproducibility and was more accurate in characterizing liver cirrhosis compared with liver ADC alone
Patel et al. <sup>[35]</sup>	30	Cirrhotic liver returned lower ADC values compared with normal liver
Sandrasegaran et al. <sup>[78]</sup>	78	ADC value of cirrhotic liver lower than normal liver. However, ADC was not able to distinguish early stages of fibrosis (METAVIR score 2 or less)
Bülow et al. <sup>[79]</sup>	95	ADC values are less reliable in the presence of hepatic fat or iron infiltration
Tosun et al. <sup>[80]</sup>	37	ADC values of cirrhotic and inflammatory liver were less than normal liver
Kovač et al. <sup>[81]</sup>	45	Transient elastography was more accurate than ADC for the evaluation of the severity of liver fibrosis
Bakan et al. <sup>[82]</sup>	59	ADC of cirrhotic liver was lower than normal liver
Bonekamp S et al. <sup>[83]</sup>		ADC inversely correlated with severity of liver fibrosis
Soylu et al. <sup>[84]</sup>	55	No correlation found between ADC and fibrosis stage
Mwangi et al. <sup>[85]</sup>	17	ADC values was higher in confluent fibrosis compared with background cirrhotic liver
Taouli et al. <sup>[29]</sup>	23	ADC values reduced in liver inflammation and fibrosis
Wang et al. <sup>[86]</sup>	14	MR elastography showed a higher diagnostic accuracy for staging liver fibrosis compared with ADC values
Watanabe et al. <sup>[87]</sup>	114	Hepatocyte-phase gadoxetate disodium-enhanced MR imaging was more reliable for staging liver cirrhosis compared with ADC values
Koinuma et al. <sup>[30]</sup>	31	Inverse correlation between ADC values and fibrosis scores
Luciani et al. <sup>[36]</sup>	12	ADC and perfusion-sensitive diffusion parameters are lower in liver fibrosis compared with normal liver

evaluate other diffusion quantitative metrics derived by different diffusion models to improve diagnostic performance.

### *Steatosis*

Hepatic steatosis or fatty infiltration can progress to hepatitis and eventually to cirrhosis. The accepted standard for diagnosis is liver biopsy, although non-invasive MRI using fat–water separation sequences is becoming accepted as a non-invasive method of diagnosis and means of assessing the hepatic fat fraction. Significant hepatic steatosis has been shown to lower hepatic ADC values. One probable explanation for this observation is that protons associated with intra- and extracellular fat have reduced diffusivity, thus resulting in a lower ADC compared with normal parenchyma<sup>[40]</sup>. A recent study by Poyraz et al.<sup>[41]</sup> showed a significant ADC reduction in patients with a hepatic fat fraction of greater than 5% and demonstrated an inverse relationship between ADC and hepatic fat fraction. However, an earlier study found no correlation between ADC values and hepatic fat fraction, although MR spectroscopy and dual-echo chemical shift imaging in the same population showed good correlation with hepatic fat fraction<sup>[42]</sup>.

### *Haemochromatosis*

In patients with haemochromatosis, the high parenchymal iron content induces susceptibility artefacts that result in low signal intensity on diffusion sequences and spuriously low ADC values. These susceptibility artefacts can also lead to obscuration of smaller focal liver lesions,

and disease evaluation in the presence of iron overload in the liver should be interpreted with caution.

## **Applications of liver DW-MRI**

Application of a small diffusion weighting ( $b < 50\text{--}150\text{ s mm}^{-2}$ ) nulls the intrahepatic vascular signal resulting in black-blood images that improve the detection of focal liver lesions while maintaining a high SNR (Fig. 2)<sup>[13,43–47]</sup>. The use of higher  $b$  values ( $>500\text{ s mm}^{-2}$ ) facilitates liver lesion characterization, helping to distinguish between cystic and solid lesions<sup>[48,49]</sup>. However, differentiation between different solid lesions is difficult based on visual assessment because these lesions, whether benign or malignant, demonstrate impeded diffusion on the high  $b$  value images. Hence, further lesion characterization by DW-MRI could be aided by evaluating the ADC map in conjunction with the morphologic sequences.

### *Focal liver lesion detection*

A substantial number of studies have compared DW-MRI with T2-weighted imaging or contrast-enhanced MRI for the detection of focal liver lesions (Tables 3 and 4). These studies have shown improved liver lesion detection on diffusion sequences<sup>[13,43,46,47,50,51]</sup> compared with conventional T2-weighted MRI or even contrast-enhanced MRI.

Compared with T2-weighted MRI, the use of low  $b$  values to generate black-blood images has been shown to result in comparable image quality but improved lesion detection<sup>[13,45,47]</sup>, particularly for lesions less

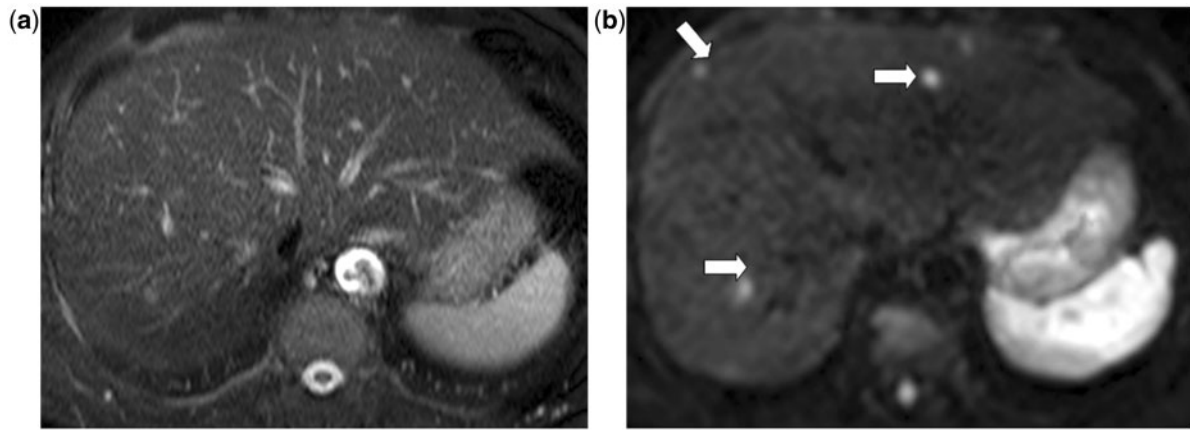


**Figure 2** A 56-year-old man with a history of colorectal cancer. (a) T2-weighted and (b)  $b = 100 \text{ s mm}^{-2}$  image of the liver. Liver metastases (arrows) appear more conspicuous on the diffusion-weighted image as the high signal from the intrahepatic vasculature is suppressed by applying diffusion weighting.

**Table 3** Studies comparing DWI with T2-weighted imaging for the detection of focal liver lesions

Year	Authors	No. of patients	Findings
2011	Yang et al. <sup>[88]</sup>	45	Improved detection of malignant hepatic lesions using DWI
2009	Coenegrachts et al. <sup>[89]</sup>	25	Non-contrast single-shot echo-planar imaging-DWI best for lesion detection
2008	Parikh et al. <sup>[13]</sup>	53	DWI better than T2-weighted imaging for lesion detection
2008	Bruegel et al. <sup>[90]</sup>	52	DWI had highest sensitivity for lesion detection
2008	Zech et al. <sup>[43]</sup>	20	Higher detection rate using DWI
2008	Goshima et al. <sup>[91]</sup>	76	$b = 100$ best for lesion detection
2007	Coenegrachts et al. <sup>[92]</sup>	24	DWI increased lesion conspicuity
1998	Ichikawa et al. <sup>[93]</sup>	46	Increased detection of malignancy using DWI
1998	Okada et al. <sup>[46]</sup>	48	Improved lesion detection using DWI

**Table 4** Studies comparing DWI with contrast-enhanced MRI for the detection of focal liver lesions

Year	Authors	No. of patients	Comparison	Findings
2012	Song et al. <sup>[94]</sup>	158	Gd-EOB-DTPA	No difference in diagnostic accuracy for DWI performed with or without contrast enhancement
2012	Kim et al. <sup>[95]</sup>	86	Gd-EOB-DTPA	Combined DWI and Gd-EOB-DTPA imaging showed higher accuracy and sensitivity
2012	Holzepfel et al. <sup>[55]</sup>	36	Gd-EOB-DTPA	Combined DWI and Gd-EOB-DTPA improved detection of lesions <1 cm in diameter
2011	Chung et al. <sup>[96]</sup>	47	Gd-EOB-DTPA	Combination of DWI and Gd-EOB-DTPA showed higher accuracy for detection of metastases
2012	Koh et al. <sup>[8]</sup>	72	Gd-EOB-DTPA	Improves diagnostic accuracy using combination of DWI and Gd-EOB-DTPA enhanced imaging
2011	Löwenthal et al. <sup>[97]</sup>	73	Gd-EOB-DTPA	DWI good for detecting small metastases
2010	Shimada et al. <sup>[98]</sup>	45	Gd-EOB-DTPA	Gd-EOB-DTPA MRI showed higher accuracy
2009	Coenegrachts et al. <sup>[89]</sup>	25	SPIO, TSE T2W	Non-contrast single-shot echo-planar imaging-DWI best for lesion detection
2006	Nasu et al. <sup>[99]</sup>	24	SPIO	DWI + T1/T2 resulted in highest detection rate compared with SPIO-enhanced imaging
2008	Koh et al. <sup>[54]</sup>	33	Mn-DPDP T1W	Adding DWI to Mn-DPDP resulted in highest detection rate

DTPA, diethylenetriaminepentaacetic acid; EOB, ethoxybenzyl; Mn-DPDP, mangafodipir trisodium; SPIO, superparamagnetic iron oxide; TSE, turbo spin-echo.

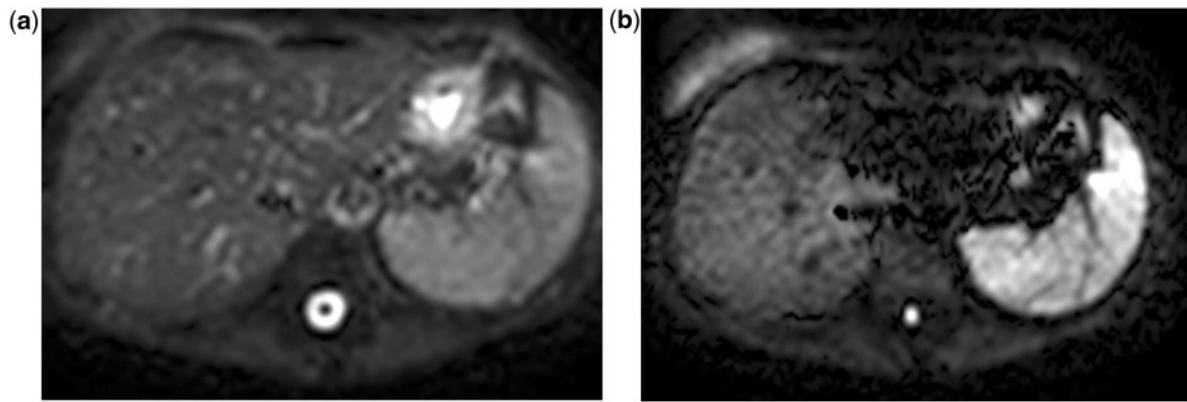


**Figure 3** Artefacts over the left lobe of the liver. Diffusion-weighted (a)  $b = 0 \text{ s mm}^{-2}$  and (b)  $b = 500 \text{ s mm}^{-2}$  images. On the higher  $b$  value image (b), note substantial artefacts over the left lobe due to cardiac motion, which can obscure lesions located in this area.

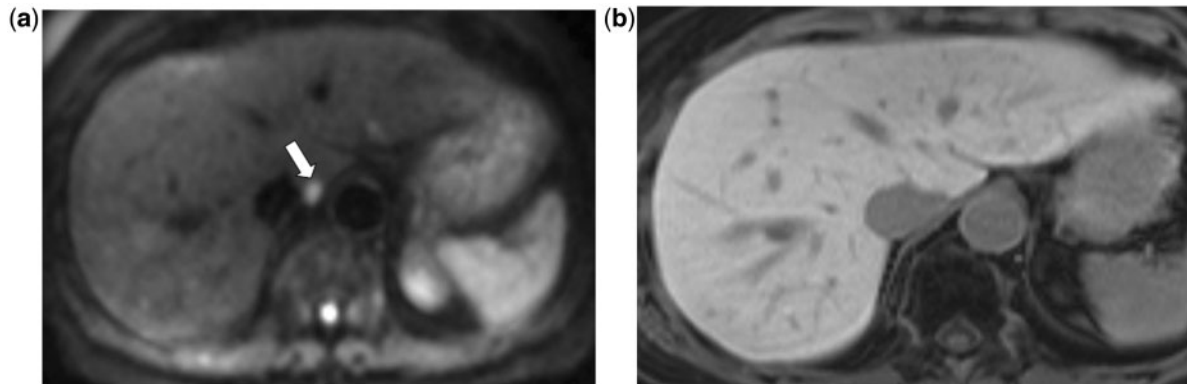


**Figure 4** Liver metastasis mimicking intrahepatic vasculature on Gd-EOB-DTPA-enhanced imaging. A 48 year-old man with colorectal cancer. (a)  $b = 750 \text{ s mm}^{-2}$  image shows high-signal metastasis in the caudate lobe of the liver adjacent to the inferior vena cava (arrow). (b) The lesion is poorly seen and cannot be distinguished from the intrahepatic vasculature, which also appears hypointense relative to the liver in the hepatocellular phase of contrast enhancement.

than or equal to 1 cm in diameter<sup>[51]</sup>, for lesions lying adjacent to blood vessels and for those located in the right hepatic lobe<sup>[13]</sup>. Improvement in lesion detection with DW-MRI can be explained by improved lesion to background image contrast using low  $b$  value (or black-blood) images, which helps to differentiate small metastases from intrahepatic vasculature<sup>[47]</sup>. However, lesions in the sub-diaphragmatic right lobe of the liver, as well as the sub-cardiac region in the left hepatic lobe may be obscured due to motion-induced artefacts (Fig. 3).

Other studies have compared focal liver lesion detection on DW-MRI with contrast-enhanced (superparamagnetic iron oxide, low molecular gadolinium chelates, gadoxetic acid and mangafodipir trisodium) examinations. These studies (Table 3) demonstrated that DW-MRI has a high sensitivity and specificity for the detection of liver metastases<sup>[44,52–54]</sup>. Even with the use of the liver-specific contrast medium (Gd-EOB-DTPA), it was the combination of hepatocellular phase T1-weighted

imaging and DW-MR images that resulted in the highest diagnostic accuracy, increasing sensitivity without sacrificing specificity<sup>[54,55]</sup>. This is because combining these techniques maximizes the advantages of each while minimizing their disadvantages. DW-MRI improves the detection of small metastases that may mimic small blood vessels on the hepatocellular phase of Gd-EOB-DTPA-enhanced imaging (Fig. 4), whereas contrast-enhanced images are more useful in the sub-diaphragmatic and sub-cardiac liver regions, which are prone to DW-MRI artefacts<sup>[8]</sup>. When DW-MRI was performed after the administration of superparamagnetic iron oxide contrast medium, lesion detection was also improved by suppression of background liver signal<sup>[56]</sup>.

#### *Focal liver lesion characterization*

Although DW-MRI can be used to distinguish solid from cystic lesions, this usually does not pose a significant

**Table 5** Reported ADC values of benign versus malignant hepatic lesions

	Namimoto et al. <sup>[9]</sup>	Kim et al. <sup>[49]</sup>	Taouli et al. <sup>[48]</sup>	Bruegel et al. <sup>[12]</sup>	Goutsoyianni et al. <sup>[14]</sup>	Parikh et al. <sup>[13]</sup>	Cieszanowski et al. <sup>[100]</sup>
No of patients	51	126	66	102	38	53	73
<i>b</i> value (s mm <sup>-2</sup> )	30, 1200	<846	<500	50, 300, 600	0, 50, 500, 1000	0, 50, 500	50, 400, 800
<b>ADC values (mm s<sup>-1</sup>)</b>							
Normal liver	0.69	1.02	1.83	1.24	1.25–1.31	Not applicable	Not applicable
Metastases	1.15	1.06–1.11	0.94	1.22	0.99	1.50	1.05
HCCs	0.99	0.97–1.28	1.33	1.05	1.38	1.31	0.94
Haemangiomas	1.95	2.04–2.10	2.95	1.92	1.90	2.04	1.55
Cysts	3.05	2.91–3.03	3.63	3.02	2.55	2.54	2.45
Focal nodular hyperplasia/adenomas	Not applicable	Not applicable	1.75	1.40	Not applicable	1.49	1.18
ADC cut-off to distinguish benign from malignant	Not applicable	1.60	1.50	1.63	1.47	1.60	1.25
Sensitivity (%)	Not applicable	98	84	90	100	74	79
Specificity (%)	Not applicable	80	89	86	100	77	83

diagnostic challenge even on conventional morphologic imaging. Characterization of solid hepatic lesions is usually more challenging due to the substantial overlap in their conventional morphologic appearance, DW-MRI appearances and the ADC values between benign and malignant lesions. However, benign lesions have been shown to have higher (i.e. less impeded) ADC values than malignant lesions<sup>[9,12,13,48,49,57]</sup> (Table 5). From the published literature, it would seem that a threshold value of approximately  $1.7 \times 10^{-3} \text{ mm}^2 \text{ s}^{-1}$  has a fairly high diagnostic sensitivity and specificity for differentiating benign from malignant focal disease<sup>[9,10,12–14,48]</sup>. Of the benign solid lesions, hepatic haemangiomas have the highest ADC value, typically higher than the adjacent liver parenchyma, which can be ascribed to the T2 shine-through effect (Fig. 5).

When comparing or interpreting ADC values, it is important to be aware of the method of ADC calculation and to compare with values obtained using similar techniques to avoid misinterpretation. For example, ADC values calculated using or including low *b* values ( $\leq 100 \text{ s mm}^{-2}$ ) are higher because perfusional effects are included<sup>[49,58]</sup>. Consensus recommendations suggest that the omission of *b* = 0 and calculation using a range of higher and lower *b* values<sup>[7]</sup> may be practical to avoid measurement uncertainty that may arise from variations in the flow-sensitive components of the diffusion measurements.

Quantitative ADC measurements can be used to aid focal liver lesion characterization, but it may be difficult to confidently describe a lesion as benign or malignant based on ADC values alone, due to the considerable overlap between groups of hepatic pathologies. In one recent study, benign solid hepatic lesions, such as focal nodular hyperplasia and adenomas, were found to have similar ADC values compared with malignant disease, such as metastases and hepatocellular carcinoma<sup>[59]</sup>. Mucinous metastatic deposits (e.g. from ovarian or colorectal primaries) can mimic benign lesions such as simple

cysts and haemangiomas. For these reasons, one should not rely on ADC values as the sole basis for disease characterization. It is important to take into account the clinical background (e.g. histology of primary tumour), temporal context (i.e. untreated metastatic deposits will show an interval increase in size) and other available imaging before making a radiologic diagnosis.

In a recently published study, Battal et al.<sup>[60]</sup> suggest that simply using visual assessment of source DW-MR images performed using *b*0 and *b*800 allows detection and differentiation of focal liver lesions. All focal liver lesions showed hyperintensity on the *b*0 images, benign lesions tended to become isointense or hypointense on *b*800 images, and malignant lesions remained hyperintense. In their study, qualitative visual assessment performed better than quantitative ADC measurement with sensitivities of 100% and 100%, and specificities of 92.2% and 89.3%, respectively. However, in that study, few lesions were haemangiomas, which could have confounded the results.

### *Hepatocellular carcinoma and assessment of tumour grade*

The cirrhotic liver shows impeded diffusion and is associated with lower ADC values, which reduces the contrast between hepatocellular carcinoma and the background cirrhotic liver. Histopathologic grade is one of the important prognostic indicators in hepatocellular carcinoma (HCC). An early study by Nasu et al.<sup>[61]</sup> showed that the signal intensity of lesions on the diffusion acquisition tended to increase as the grade of tumour increased in 125 surgically resected hypervascular HCCs. Although some studies showed that well-differentiated HCCs returned higher ADC values, other studies found no correlation between tumour grade and the mean ADC value, and there was a large overlap between grades<sup>[61]</sup>. More recent data from Nishie et al.<sup>[62]</sup> suggests that minimum ADC could be useful

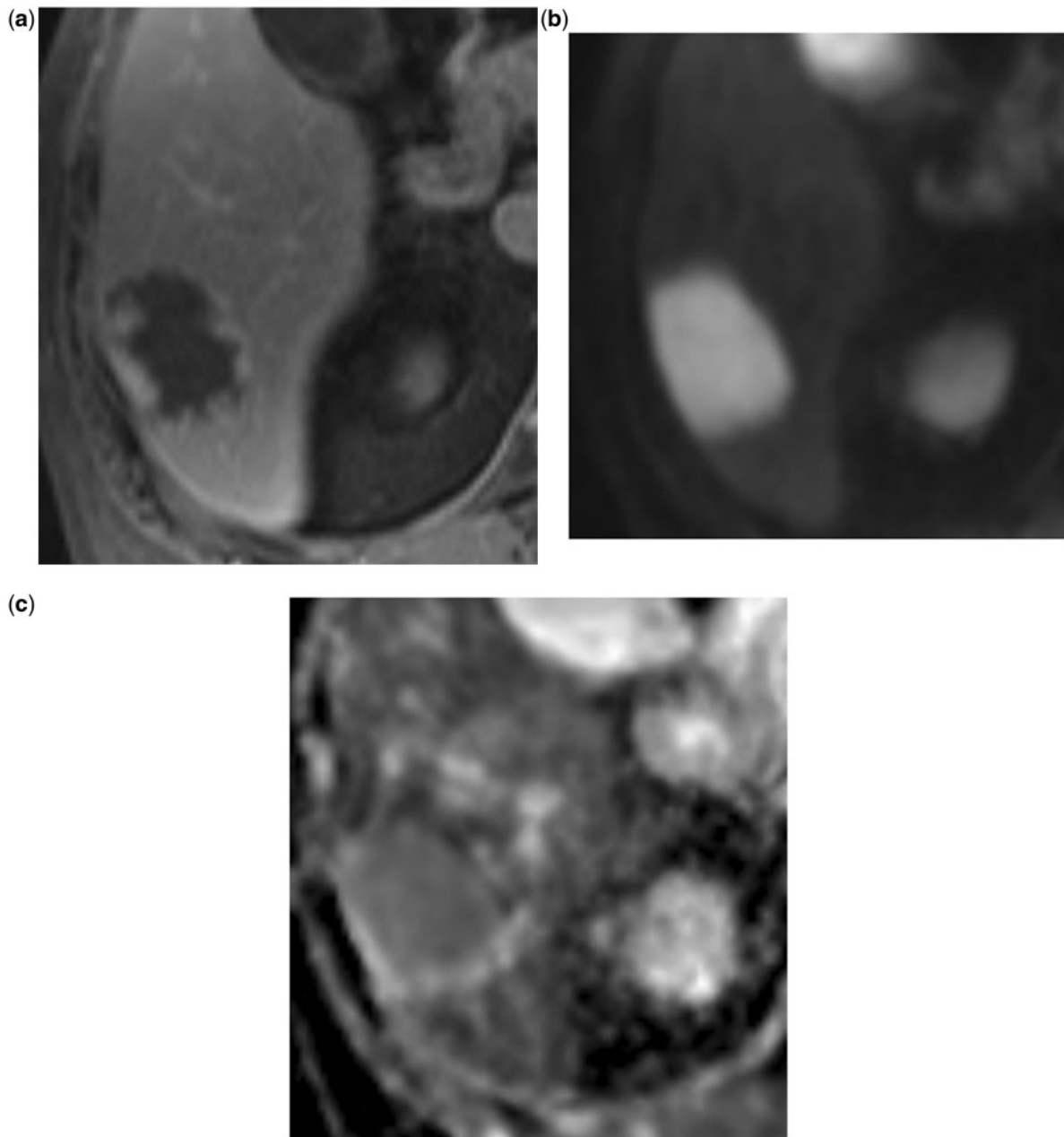


**Figure 5** A 55 year-old woman with a history of breast cancer. (a) T1-weighted arterial phase after Gd-DOTA contrast administration shows peripheral nodular enhancement of the lesion in the right lobe of the liver. (b) The lesion shows persistent high signal on the high  $b$ -value image ( $b = 750 \text{ s mm}^{-2}$ ), due to the long T2 relaxation time (T2 shine-through). (c) The lesion returns a typical ADC value higher than the adjacent liver on the ADC map. Appearances are in keeping with a hepatic haemangioma.

in detecting poorly differentiated components of the tumour and that application of an ADC cut-off at  $0.972 \times 10^{-3} \text{ mm}^2 \text{ s}^{-1}$  distinguished moderately to poorly and poorly differentiated HCCs with a sensitivity of 73.1% and specificity of 72.9%. Similar results were obtained by Nakanishi et al.<sup>[63]</sup> who showed that minimum ADC predicted histologic grade in HCC and early tumour recurrence (<6 months after hepatectomy).

However, care is needed to ensure minimum ADC measurements are not confounded by image artefacts, which can lead to spuriously low values.

In addition, recent studies have found that combining DW-MRI with conventional contrast-enhanced MRI can improve the detection of HCC, compared with contrast-enhanced MRI on its own<sup>[64]</sup> (Fig. 6).

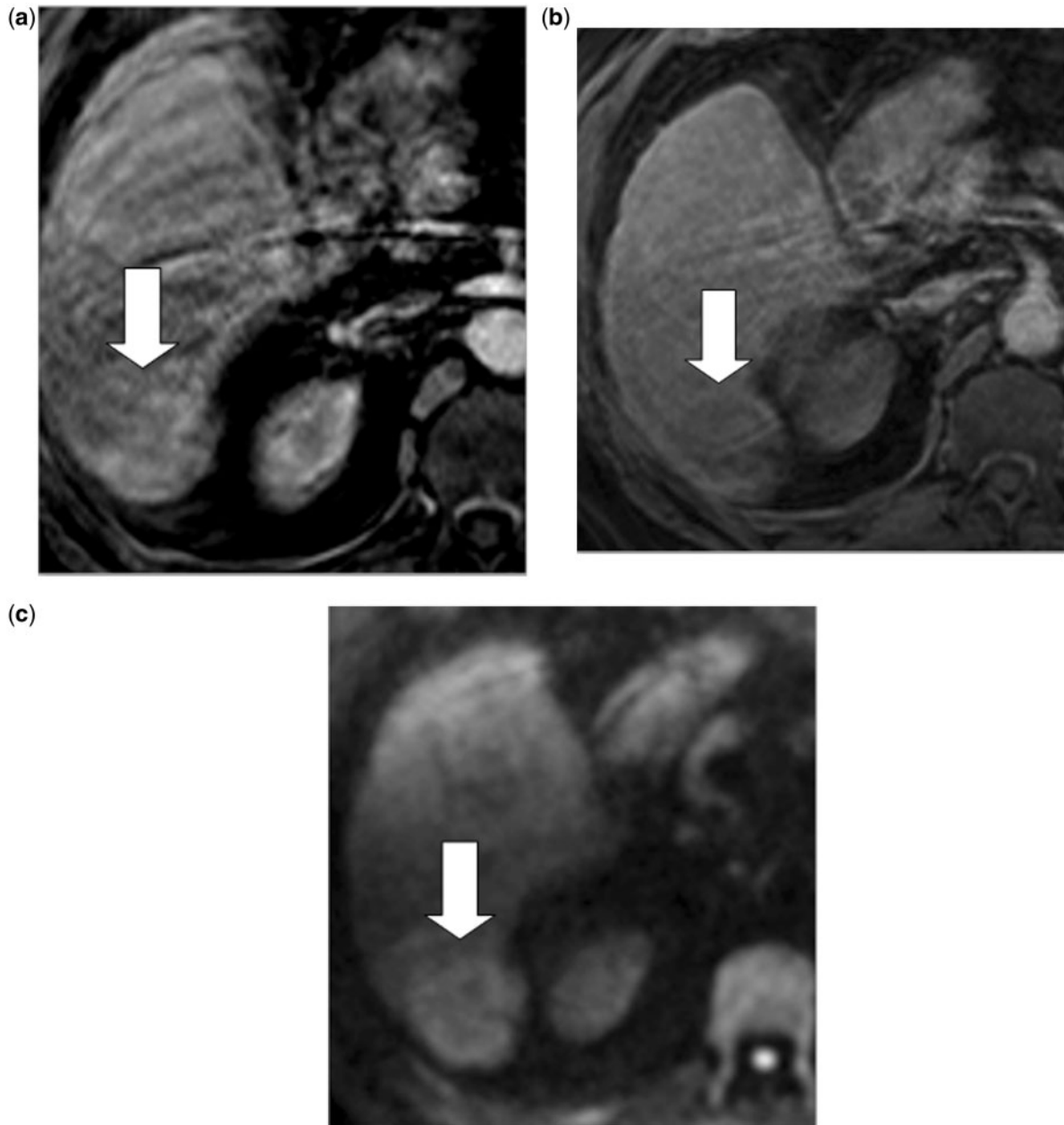


**Figure 6** Typical imaging appearances of HCC. In cirrhotic liver, HCC (arrows) typically (a) demonstrates hyperenhancement in the arterial phase of low molecular weight Gd contrast-enhanced imaging; (b) appears relatively hypointense to liver in the portovenous or interstitial phase of contrast enhancement (washout) and (c) shows impeded diffusion on diffusion-weighted imaging ( $b = 500 \text{ s mm}^{-2}$ ).

#### *Tumour response to treatment*

The prediction and detection of therapeutic response and the detection of residual disease are paramount in oncologic imaging. DW-MRI is increasingly being used as a means of assessing tumour response to various treatment modalities (e.g. chemotherapy, radiotherapy, targeted therapy, embolization and other combined treatments). The early detection of treatment responders could allow changes in therapy to minimize treatment-related toxicity and individualize management of specific tumour biology.

Tumour response is conventionally assessed by measurement of percentage reduction in tumour size after therapy (e.g. using RECIST 1.1 criteria<sup>[65]</sup>). However, changes in tumour size are insensitive to early treatment changes and may be inappropriate for monitoring the effects of novel therapeutic agents, which are frequently cytostatic (e.g. tyrosine kinase inhibitors). Studies have shown that effective tumour treatment can result in an increase in ADC value long before measureable changes in lesion size are detected<sup>[66]</sup>, and as early as 1–4 weeks from the start of therapy.

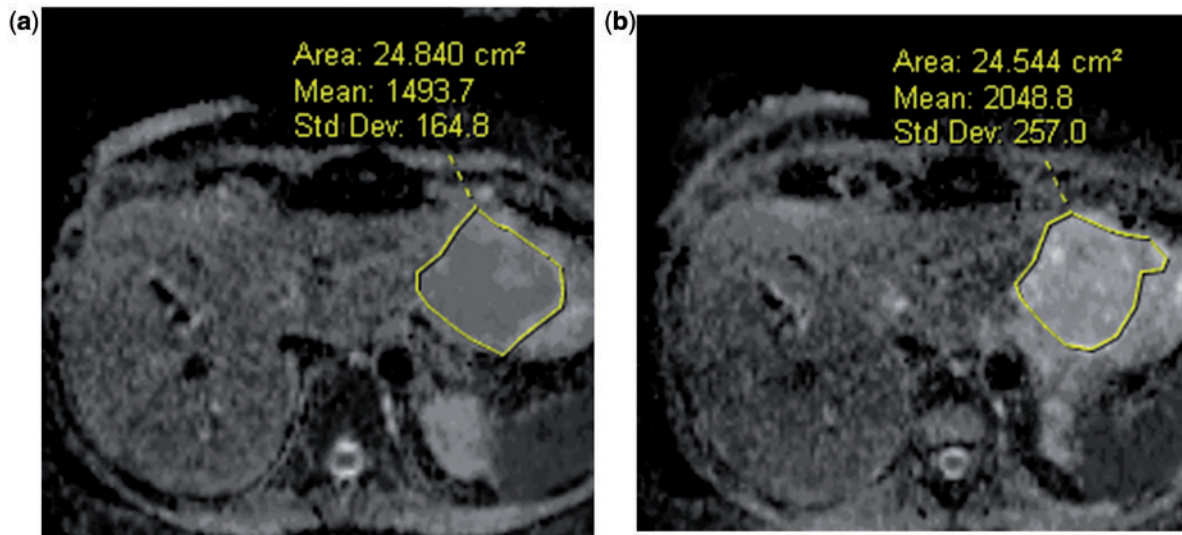


**Figure 7** A 47-year-old man with liver metastasis from a gastrointestinal stromal tumour. ADC maps obtained (a) pre-treatment and (b) at 12 weeks after that start of treatment show no significant change in tumour size (cross-sectional area). However, there was a 37% increase in the mean ADC value (pre-treatment  $ADC = 1.49 \times 10^{-3} \text{ mm}^2 \text{ s}^{-1}$ ; post-treatment  $ADC = 2.05 \times 10^{-3} \text{ mm}^2 \text{ s}^{-1}$ ) within the tumour after treatment in keeping with treatment response.

Studies have been carried out on both primary and metastatic hepatic lesions to assess treatment-related DW-MRI changes. In patients with colorectal hepatic metastases, mean lesional ADC values have been shown to increase in response to chemotherapy in those patients showing at least a partial response<sup>[67,68]</sup>, reflecting a reduction in tissue cellular density and barriers to water movement. This ADC increase was not seen in lesions that showed no change or disease progression<sup>[67]</sup>. An example of ADC increase in response to treatment in a liver metastasis is shown in Fig. 7.

Patients who are not eligible for surgery often receive locoregional therapy for liver tumours, most commonly in the form of radiofrequency ablation (RFA) and transcatheter arterial chemoembolization (TACE). DW-MRI in the follow-up of patients receiving RFA for hepatic metastases has shown promising results for the detection of local tumour progression. In 58 of 148 examinations, peripheral ablation zone hyperintensity was detected, which corresponded with local tumour progression in only 17 patients (Fig. 8). However, quantitative evaluation of these hyperintense areas showed significantly lower ADC values in those patients with tumour recurrence than in those without<sup>[69]</sup>. Several studies have evaluated the response of primary HCC to chemo- or radioembolization and have demonstrated ADC differences between viable and necrotic portions of the tumour and measurable changes with treatment<sup>[70–75]</sup>.

#### *Disease prognostication*

Prediction of which tumours will respond to treatment before onset could bring considerable clinical benefit. There are limited data available on disease

prognostication and the prediction of liver lesion response to treatment. High pre-treatment ADC values in colorectal hepatic metastases have been shown to predict a poor response to chemotherapy<sup>[67,68]</sup>, a finding that is in agreement with studies on primary rectal tumours<sup>[76]</sup>. This observation suggests that those tumours that are probably necrotic before treatment (with a resultant higher mean ADC) are more resistant to chemotherapy. These findings need to be validated in larger prospective studies but they clearly suggest a potential role for DW-MRI in disease prognostication.

### **Evolving developments in DW-MRI in the liver**

There is little doubt that DW-MRI has had an impact on the routine clinical evaluation of the liver, especially for the detection of focal liver lesions. With growing convergence in MR hardware and scanning technologies, implementing analogous imaging protocols across different imaging platforms is becoming a possibility.

As more studies are being conducted to assess the measurement reproducibility within and between MR imaging systems, it is clear that in a well-conducted study in which there is sufficient image SNR and minimal image artefact, mean ADC measurements have good reproducibility using the free-breathing fat-suppressed echo-planar spin-echo DW-MRI technique. A coefficient of repeatability as low as 10% can be achieved when whole liver tumours are analysed. In order to have confidence in the magnitude of the mean ADC change that can be reliably ascertained on individual scanners, the readers should validate the measurement reproducibility

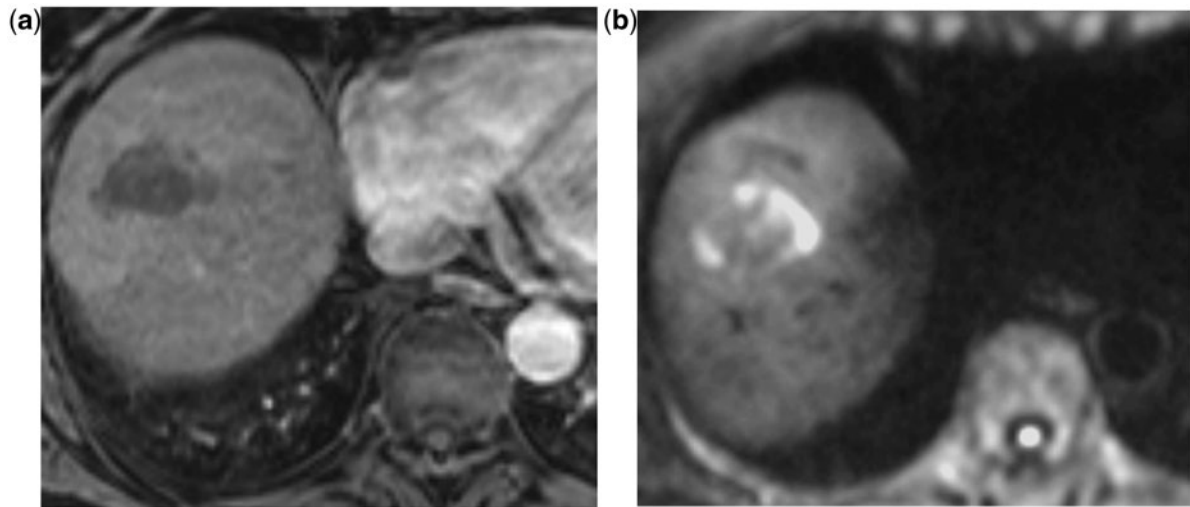


**Figure 8** A middle-aged man with previous RFA for colorectal liver metastasis in the right lobe of the liver. (a) Arterial phase Gd-DOTA-enhanced MRI shows a lesion in the right lobe with peripheral nodularity, which does not show significant enhancement. (b)  $b = 750 \text{ s mm}^{-2}$  image shows high-signal impeded diffusion in the peri-ablative zone consistent with marginal disease recurrence.

of their own diagnostic system using a particular imaging sequence on their MR scanners. Measurement reproducibility obtained from normal tissues may not be applicable to diseased states because disease tissues are typically more heterogeneous, which results in poorer measurement reproducibility compared with normal tissues<sup>[20]</sup>.

There is currently considerable interest in using a bi-exponential model by applying the principles of IVIM to the evaluation of the liver and focal liver disease. Reports in the literature suggest that it is possible to measure perfusion-sensitive parameters such as the perfusion fraction ( $f$ ) and flow-sensitive pseudodiffusion coefficient ( $D^*$ ); indeed these parameters have been found to differ between normal and diseased states. For example, studies have shown that using IVIM analysis, cirrhotic liver shows a lower perfusion fraction and pseudodiffusion coefficient. However, these findings are reported on a background of significant measurement uncertainty associated with the estimation and quantification of these parameters. In a clinical setting, it has been shown that quantification of  $f$  and  $D^*$  are associated with poor measurement reproducibility<sup>[20]</sup> (e.g. 50% or greater) and hence developments to improve the stability and reproducibility of these estimates would be important to allow the IVIM analysis to be robustly deployed within the clinical arena. Nevertheless, studies reported in the literature suggest that using these additional diffusion parameters could be helpful in a number of clinical scenarios.

## Conclusions

DW-MRI is now available on most commercial MRI platforms and is routinely incorporated into standard liver MR imaging protocols in many departments. It is

particularly useful in patients who tolerate gadolinium-based contrast agents where DW-MRI has the potential to be an alternative contrast-enhanced technique.

There are convincing data available to show that DW-MRI contributes to focal liver lesion detection and the assessment of treatment response. When used in conjunction with morphologic sequences, the mean ADC values act as an adjunct to lesion characterization. Although DW-MRI has been used for the evaluation of liver fibrosis, the sensitivity of the technique to early fibrosis appears limited, and more research is needed to optimize the measurement reproducibility of quantitative parameters derived by IVIM analysis before they can be robustly and meaningfully deployed in the clinical arena.

## Conflict of interest

The authors have no conflicts of interest to declare.

## References

- [1] Grobner T. Gadolinium—a specific trigger for the development of nephrogenic fibrosing dermopathy and nephrogenic systemic fibrosis? *Nephrol Dial Transplant* 2006; 21: 1104–1108. doi:10.1093/ndt/gfk062. PMID:16431890.
- [2] Marckmann P, Skov L, Rossen K, et al. Nephrogenic systemic fibrosis: suspected causative role of gadodiamide used for contrast-enhanced magnetic resonance imaging. *J Am Soc Nephrol* 2006; 17: 2359–2362. doi:10.1681/ASN.2006060601. PMID:16885403.
- [3] Sadowski EA, Bennett LK, Chan MR, et al. Nephrogenic systemic fibrosis: risk factors and incidence estimation. *Radiology* 2007; 243: 148–157. doi:10.1148/radiol.2431062144. PMID:17267695.
- [4] Thomsen HS, Marckmann P, Logager VB. Update on nephrogenic systemic fibrosis. *Magn Reson Imaging Clin North Am* 2008; 16: 551–560, vii. doi:10.1016/j.mric.2008.07.011.

- [5] Nicholson C, Phillips JM. Ion diffusion modified by tortuosity and volume fraction in the extracellular microenvironment of the rat cerebellum. *J Physiol* 1981; 321: 225–257. PMID:7338810.
- [6] Szafer A, Zhong J, Anderson AW, Gore JC. Diffusion-weighted imaging in tissues: theoretical models. *NMR Biomed* 1995; 8: 289–296. doi:10.1002/nbm.1940080704. PMID:8739267.
- [7] Padhani AR, Liu G, Koh DM, et al. Diffusion-weighted magnetic resonance imaging as a cancer biomarker: consensus and recommendations. *Neoplasia* 2009; 11: 102–125. PMID:19186405.
- [8] Koh DM, Collins DJ, Wallace T, Chau I, Riddell AM. Combining diffusion-weighted MRI with Gd-EOB-DTPA-enhanced MRI improves the detection of colorectal liver metastases. *Br J Radiol* 2012; 85: 980–989. doi:10.1259/bjr/91771639. PMID:22167501.
- [9] Namimoto T, Yamashita Y, Sumi S, Tang Y, Takahashi M. Focal liver masses: characterization with diffusion-weighted echo-planar MR imaging. *Radiology* 1997; 204: 739–744. PMID:9280252.
- [10] Taouli B, Koh DM. Diffusion-weighted MR imaging of the liver. *Radiology* 2010; 254: 47–66. doi:10.1148/radiol.09090021. PMID:20032142.
- [11] Taouli B, Vilgrain V, Dumont E, Daire JL, Fan B, Menu Y. Evaluation of liver diffusion isotropy and characterization of focal hepatic lesions with two single-shot echo-planar MR imaging sequences: prospective study in 66 patients. *Radiology* 2003; 226: 71–78. doi:10.1148/radiol.2261011904. PMID:12511671.
- [12] Bruegel M, Holzapfel K, Gaa J, et al. Characterization of focal liver lesions by ADC measurements using a respiratory triggered diffusion-weighted single-shot echo-planar MR imaging technique. *Eur Radiol* 2008; 18: 477–485. doi:10.1007/s00330-007-0785-9. PMID:17960390.
- [13] Parikh T, Drew SJ, Lee VS, et al. Focal liver lesion detection and characterization with diffusion-weighted MR imaging: comparison with standard breath-hold T2-weighted imaging. *Radiology* 2008; 246: 812–822. doi:10.1148/radiol.2463070432. PMID:18223123.
- [14] Gourtsoyianni S, Papanikolaou N, Yarmenitis S, Maris T, Karantanis A, Gourtsoyiannis N. Respiratory gated diffusion-weighted imaging of the liver: value of apparent diffusion coefficient measurements in the differentiation between most commonly encountered benign and malignant focal liver lesions. *Eur Radiol* 2008; 18: 486–492. doi:10.1007/s00330-007-0798-4. PMID:17994317.
- [15] Kwee TC, Takahara T, Koh DM, Nievelstein RA, Luijten PR. Comparison and reproducibility of ADC measurements in breath-hold, respiratory triggered, and free-breathing diffusion-weighted MR imaging of the liver. *J Magn Reson Imaging* 2008; 28: 1141–1148. doi:10.1002/jmri.21569. PMID:18972355.
- [16] Braithwaite AC, Dale BM, Boll DT, Merkle EM. Short- and mid-term reproducibility of apparent diffusion coefficient measurements at 3.0-T diffusion-weighted imaging of the abdomen. *Radiology* 2009; 250: 459–465. doi:10.1148/radiol.2502080849. PMID:19095786.
- [17] Rosenkrantz AB, Oei M, Babb JS, Niver BE, Taouli B. Diffusion-weighted imaging of the abdomen at 3.0 Tesla: image quality and apparent diffusion coefficient reproducibility compared with 1.5 Tesla. *J Magn Reson Imaging* 2011; 33: 128–135. doi:10.1002/jmri.22395. PMID:21182130.
- [18] Kim SY, Lee SS, Byun JH, et al. Malignant hepatic tumors: short-term reproducibility of apparent diffusion coefficients with breath-hold and respiratory-triggered diffusion-weighted MR imaging. *Radiology* 2010; 255: 815–823. doi:10.1148/radiol.10091706. PMID:20501719.
- [19] Malyarenko D, Galban CJ, Londy FJ, et al. Multi-system repeatability and reproducibility of apparent diffusion coefficient measurement using an ice-water phantom. *J Magn Reson Imaging* 2012; doi:10.1002/jmri.23825.
- [20] Andreou A, Koh DM, Collins DJ, et al. Measurement reproducibility of perfusion fraction and pseudodiffusion coefficient derived by intravoxel incoherent motion diffusion-weighted MR imaging in normal liver and metastases. *Eur Radiol* 2013; 23: 428–434. doi:10.1007/s00330-012-2604-1. PMID:23052642.
- [21] Colagrande S, Pasquinelli F, Mazzoni LN, Belli G, Virgili G. MR-diffusion weighted imaging of healthy liver parenchyma: repeatability and reproducibility of apparent diffusion coefficient measurement. *J Magn Reson Imaging* 2010; 31: 912–920. doi:10.1002/jmri.22117. PMID:20373436.
- [22] Koh DM, Blackledge M, Collins DJ, et al. Reproducibility and changes in the apparent diffusion coefficients of solid tumours treated with combretastatin A4 phosphate and bevacizumab in a two-centre phase I clinical trial. *Eur Radiol* 2009; 19: 2728–2738. doi:10.1007/s00330-009-1469-4. PMID:19547986.
- [23] Maharaj B, Maharaj RJ, Leary WP, et al. Sampling variability and its influence on the diagnostic yield of percutaneous needle biopsy of the liver. *Lancet* 1986; 1: 523–525. PMID:2869260.
- [24] Ratziu V, Charlotte F, Heurtier A, et al. Sampling variability of liver biopsy in nonalcoholic fatty liver disease. *Gastroenterology* 2005; 128: 1898–1906. doi:10.1053/j.gastro.2005.03.084. PMID:15940625.
- [25] Bravo AA, Sheth SG, Chopra S. Liver biopsy. *N Engl J Med* 2001; 344: 495–500. doi:10.1056/NEJM200102153440706. PMID:11172192.
- [26] Piccinino F, Sagnelli E, Pasquale G, Giusti G. Complications following percutaneous liver biopsy. A multicentre retrospective study on 68,276 biopsies. *J Hepatol* 1986; 2: 165–173. doi:10.1016/S0168-8278(86)80075-7. PMID:3958472.
- [27] Amano Y, Kumazaki T, Ishihara M. Single-shot diffusion-weighted echo-planar imaging of normal and cirrhotic livers using a phased-array multicoil. *Acta Radiol* 1998; 39: 440–442. PMID:9685834.
- [28] Taouli B, Chouli M, Martin AJ, Qayyum A, Coakley FV, Vilgrain V. Chronic hepatitis: role of diffusion-weighted imaging and diffusion tensor imaging for the diagnosis of liver fibrosis and inflammation. *J Magn Reson Imaging* 2008; 28: 89–95. doi:10.1002/jmri.21227. PMID:18581382.
- [29] Taouli B, Tolia AJ, Losada M, et al. Diffusion-weighted MRI for quantification of liver fibrosis: preliminary experience. *AJR Am J Roentgenol* 2007; 189: 799–806. doi:10.2214/AJR.07.2086. PMID:17885048.
- [30] Koinuma M, Ohashi I, Hanafusa K, Shibuya H. Apparent diffusion coefficient measurements with diffusion-weighted magnetic resonance imaging for evaluation of hepatic fibrosis. *J Magn Reson Imaging* 2005; 22: 80–85. doi:10.1002/jmri.20344. PMID:15971188.
- [31] Girometti R, Furlan A, Bazzocchi M, et al. Diffusion-weighted MRI in evaluating liver fibrosis: a feasibility study in cirrhotic patients. *Radiol Med* 2007; 112: 394–408. doi:10.1007/s11547-007-0149-1. PMID:17440695.
- [32] Lewin M, Poujol-Robert A, Boelle PY, et al. Diffusion-weighted magnetic resonance imaging for the assessment of fibrosis in chronic hepatitis C. *Hepatology* 2007; 46: 658–665. doi:10.1002/hep.21747. PMID:17663420.
- [33] Naganawa S, Kawai H, Fukatsu H, et al. Diffusion-weighted imaging of the liver: technical challenges and prospects for the future. *Magn Reson Med Sci* 2005; 4: 175–186. doi:10.2463/mrms.4.175. PMID:16543702.
- [34] Aube C, Racineux PX, Lebigot J, et al. [Diagnosis and quantification of hepatic fibrosis with diffusion weighted MR imaging: preliminary results]. *J Radiol* 2004; 85: 301–306. doi:10.1016/S0221-0363(04)97582-8. PMID:15192522.
- [35] Patel J, Sigmund EE, Rusinek H, Oei M, Babb JS, Taouli B. Diagnosis of cirrhosis with intravoxel incoherent motion diffusion MRI and dynamic contrast-enhanced MRI alone and in combination: preliminary experience. *J Magn Reson Imaging* 2010; 31: 589–600. doi:10.1002/jmri.22081. PMID:20187201.
- [36] Luciani A, Vignaud A, Cavet M, et al. Liver cirrhosis: intravoxel incoherent motion MR imaging—pilot study. *Radiology* 2008; 249: 891–899. doi:10.1148/radiol.2493080080. PMID:19011186.

- [37] Fujimoto K, Tonan T, Azuma S, et al. Evaluation of the mean and entropy of apparent diffusion coefficient values in chronic hepatitis C: correlation with pathologic fibrosis stage and inflammatory activity grade. *Radiology* 2011; 258: 739–748. doi:10.1148/radiol.10100853. PMID:21248235.
- [38] Benedict RH, Bruce J, Dwyer MG, et al. Diffusion-weighted imaging predicts cognitive impairment in multiple sclerosis. *Mult Scler* 2007; 13: 722–730. doi:10.1177/1352458507075592. PMID:17613599.
- [39] Tavazzi E, Dwyer MG, Weinstock-Guttman B, et al. Quantitative diffusion weighted imaging measures in patients with multiple sclerosis. *Neuroimage* 2007; 36: 746–754. doi:10.1016/j.neuroimage.2007.03.056. PMID:17498974.
- [40] Wignall O, Scurr E, Collins D, Thng C-H, Koh DM. Hepatic steatosis results in a reduction in the apparent diffusion coefficient (ADC) of liver parenchyma. Abstract. 2008 Conference Proceedings for the ISMRM 16th Scientific Meeting Exhibition.
- [41] Poyraz AK, Onur MR, Kocakoc E, Ogur E. Diffusion-weighted MRI of fatty liver. *J Magn Reson Imaging* 2012; 35: 1108–1111. doi:10.1002/jmri.23519. PMID:22170763.
- [42] d'Assignies G, Ruel M, Khiat A, et al. Noninvasive quantitation of human liver steatosis using magnetic resonance and bioassay methods. *Eur Radiol* 2009; 19: 2033–2040. doi:10.1007/s00330-009-1351-4. PMID:19280194.
- [43] Zech CJ, Herrmann KA, Dietrich O, Horger W, Reiser MF, Schoenberg SO. Black-blood diffusion-weighted EPI acquisition of the liver with parallel imaging: comparison with a standard T2-weighted sequence for detection of focal liver lesions. *Invest Radiol* 2008; 43: 261–266. doi:10.1097/RLI.0b013e31816200b5. PMID:18340250.
- [44] Coenegrachts K, Orlent H, ter Beek L, et al. Improved focal liver lesion detection: comparison of single-shot spin-echo echoplanar and superparamagnetic iron oxide (SPIO)-enhanced MRI. *J Magn Reson Imaging* 2008; 27: 117–124. doi:10.1002/jmri.21247. PMID:18050350.
- [45] van den Bos IC, Hussain SM, Krestin GP, Wielopolski PA. Liver imaging at 3.0 T: diffusion-induced black-blood echo-planar imaging with large anatomic volumetric coverage as an alternative for specific absorption rate-intensive echo-train spin-echo sequences: feasibility study. *Radiology* 2008; 248: 264–271. doi:10.1148/radiol.2481070034. PMID:18566178.
- [46] Okada Y, Ohtomo K, Kiryu S, Sasaki Y. Breath-hold T2-weighted MRI of hepatic tumors: value of echo planar imaging with diffusion-sensitizing gradient. *J Comput Assist Tomogr* 1998; 22: 364–371. doi:10.1097/00004728-199805000-00005. PMID:9606375.
- [47] Hussain SM, De Becker J, Hop WC, Dwarkasing S, Wielopolski PA. Can a single-shot black-blood T2-weighted spin-echo echo-planar imaging sequence with sensitivity encoding replace the respiratory-triggered turbo spin-echo sequence for the liver? An optimization and feasibility study. *J Magn Reson Imaging* 2005; 21: 219–229. doi:10.1002/jmri.20269. PMID:15723376.
- [48] Taouli B, Vilgrain V, Dumont E, Daire JL, Fan B, Menu Y. Evaluation of liver diffusion isotropy and characterization of focal hepatic lesions with two single-shot echo-planar MR imaging sequences: prospective study in 66 patients. *Radiology* 2003; 226: 71–78. doi:10.1148/radiol.2261011904. PMID:12511671.
- [49] Kim T, Murakami T, Takahashi S, Hori M, Tsuda K, Nakamura H. Diffusion-weighted single-shot echoplanar MR imaging for liver disease. *AJR Am J Roentgenol* 1999; 173: 393–398. doi:10.2214/ajr.173.2.10430143. PMID:10430143.
- [50] Coenegrachts K, Delanote J, ter Beek L, et al. Improved focal liver lesion detection: comparison of single-shot diffusion-weighted echoplanar and single-shot T2 weighted turbo spin echo techniques. *Br J Radiol* 2007; 80: 524–531. doi:10.1259/bjr/33156643. PMID:17510250.
- [51] Bruegel M, Gaa J, Waldt S, et al. Diagnosis of hepatic metastasis: comparison of respiration-triggered diffusion-weighted echoplanar MRI and five t2-weighted turbo spin-echo sequences. *AJR Am J Roentgenol* 2008; 191: 1421–1429. doi:10.2214/AJR.07.3279. PMID:18941080.
- [52] Nasu K, Kuroki Y, Nawano S, et al. Hepatic metastases: diffusion-weighted sensitivity-encoding versus SPIO-enhanced MR imaging. *Radiology* 2006; 239: 122–130. doi:10.1148/radiol.2383041384. PMID:16493012.
- [53] Low RN, Gurney J. Diffusion-weighted MRI (DWI) in the oncology patient: value of breathhold DWI compared to unenhanced and gadolinium-enhanced MRI. *J Magn Reson Imaging* 2007; 25: 848–858. doi:10.1002/jmri.20864. PMID:17335018.
- [54] Koh DM, Brown G, Riddell AM, et al. Detection of colorectal hepatic metastases using MnDPDP MR imaging and diffusion-weighted imaging (DWI) alone and in combination. *Eur Radiol* 2008; 18: 903–910. doi:10.1007/s00330-007-0847-z. PMID:18193234.
- [55] Holzapfel K, Eiber MJ, Fingerle AA, Bruegel M, Rummeny EJ, Gaa J. Detection, classification, and characterization of focal liver lesions: value of diffusion-weighted MR imaging, gadoteric acid-enhanced MR imaging and the combination of both methods. *Abdom Imaging* 2012; 37: 74–82. doi:10.1007/s00261-011-9758-1. PMID:21597893.
- [56] Kiryu S, Watanabe M, Kabasawa H, Akahane M, Aoki S, Ohtomo K. Evaluation of super paramagnetic iron oxide-enhanced diffusion-weighted PROPELLER T2-fast spin echo magnetic resonance imaging: preliminary experience. *J Comput Assist Tomogr* 2006; 30: 197–200. doi:10.1097/00004728-200603000-00005. PMID:16628031.
- [57] Ichikawa T, Haradome H, Hachiya J, Nitatori T, Araki T. Diffusion-weighted MR imaging with a single-shot echoplanar sequence: detection and characterization of focal hepatic lesions. *AJR Am J Roentgenol* 1998; 170: 397–402. doi:10.2214/ajr.170.2.9456953. PMID:9456953.
- [58] Koh DM, Scurr E, Collins DJ, et al. Colorectal hepatic metastases: quantitative measurements using single-shot echo-planar diffusion-weighted MR imaging. *Eur Radiol* 2006; 16: 1898–1905. doi:10.1007/s00330-006-0201-x. PMID:16691378.
- [59] Agnello F, Ronot M, Valla DC, Sinkov R, Van Beers BE, Vilgrain V. High-b-value diffusion-weighted MR imaging of benign hepatocellular lesions: quantitative and qualitative analysis. *Radiology* 2012; 262: 511–519. doi:10.1148/radiol.11110922. PMID:22143926.
- [60] Battal B, Kocaoglu M, Akgun V, et al. Diffusion-weighted imaging in the characterization of focal liver lesions: efficacy of visual assessment. *J Comput Assist Tomogr* 2011; 35: 326–331. doi:10.1097/RCT.0b013e318216efeb. PMID:21586924.
- [61] Nasu K, Kuroki Y, Tsukamoto T, Nakajima H, Mori K, Minami M. Diffusion-weighted imaging of surgically resected hepatocellular carcinoma: imaging characteristics and relationship among signal intensity, apparent diffusion coefficient, and histopathologic grade. *AJR Am J Roentgenol* 2009; 193: 438–444. doi:10.2214/AJR.08.1424. PMID:19620441.
- [62] Nishie A, Tajima T, Asayama Y, et al. Diagnostic performance of apparent diffusion coefficient for predicting histological grade of hepatocellular carcinoma. *Eur J Radiol* 2011; 80: e29–e33. doi:10.1016/j.ejrad.2010.06.019. PMID:20619566.
- [63] Nakanishi M, Chuma M, Hige S, et al. Relationship between diffusion-weighted magnetic resonance imaging and histological tumor grading of hepatocellular carcinoma. *Ann Surg Oncol* 2012; 19: 1302–1309. doi:10.1245/s10434-011-2066-8. PMID:21927976.
- [64] Piana G, Trinquart L, Meskine N, Barrau V, Beers BV, Vilgrain V. New MR imaging criteria with a diffusion-weighted sequence for the diagnosis of hepatocellular carcinoma in chronic liver diseases. *J Hepatol* 2011; 55: 126–132. doi:10.1016/j.jhep.2010.10.023. PMID:21145857.

- [65] Eisenhauer EA, Therasse P, Bogaerts J, et al. New response evaluation criteria in solid tumours: revised RECIST guideline (version 1.1). *Eur J Cancer* 2009; 45: 228–247. doi:10.1016/j.ejca.2008.10.026. PMID:19097774.
- [66] Sharma U, Danishad KK, Seenu V, Jagannathan NR. Longitudinal study of the assessment by MRI and diffusion-weighted imaging of tumor response in patients with locally advanced breast cancer undergoing neoadjuvant chemotherapy. *NMR Biomed* 2009; 22: 104–113. doi:10.1002/nbm.1245. PMID:18384182.
- [67] Koh DM, Scurr E, Collins D, et al. Predicting response of colorectal hepatic metastasis: value of pretreatment apparent diffusion coefficients. *AJR Am J Roentgenol* 2007; 188: 1001–1008. doi:10.2214/AJR.06.0601. PMID:17377036.
- [68] Cui Y, Zhang XP, Sun YS, Tang L, Shen L. Apparent diffusion coefficient: potential imaging biomarker for prediction and early detection of response to chemotherapy in hepatic metastases. *Radiology* 2008; 248: 894–900. doi:10.1148/radiol.2483071407. PMID:18710982.
- [69] Schraml C, Schwenzer NF, Clasen S, et al. Navigator respiratory-triggered diffusion-weighted imaging in the follow-up after hepatic radiofrequency ablation-initial results. *J Magn Reson Imaging* 2009; 29: 1308–1316. doi:10.1002/jmri.21770. PMID:19418557.
- [70] Kamel IR, Bluemke DA, Ramsey D, et al. Role of diffusion-weighted imaging in estimating tumor necrosis after chemoembolization of hepatocellular carcinoma. *AJR Am J Roentgenol* 2003; 181: 708–710. doi:10.2214/ajr.181.3.1810708. PMID:12933464.
- [71] Kamel IR, Bluemke DA, Eng J, et al. The role of functional MR imaging in the assessment of tumor response after chemoembolization in patients with hepatocellular carcinoma. *J Vasc Interv Radiol* 2006; 17: 505–512. doi:10.1097/01.RVI.0000200052.02183.92. PMID:16567675.
- [72] Kamel IR, Reyes DK, Liapi E, Bluemke DA, Geschwind JF. Functional MR imaging assessment of tumor response after 90Y microsphere treatment in patients with unresectable hepatocellular carcinoma. *J Vasc Interv Radiol* 2007; 18: 49–56. doi:10.1016/j.jvir.2006.10.005. PMID:17296704.
- [73] Kamel IR, Liapi E, Reyes DK, Zahurak M, Bluemke DA, Geschwind JF. Unresectable hepatocellular carcinoma: serial early vascular and cellular changes after transarterial chemoembolization as detected with MR imaging. *Radiology* 2009; 250: 466–473. doi:10.1148/radiol.2502072222. PMID:19188315.
- [74] Chen CY, Li CW, Kuo YT, et al. Early response of hepatocellular carcinoma to transcatheter arterial chemoembolization: choline levels and MR diffusion constants—initial experience. *Radiology* 2006; 239: 448–456. doi:10.1148/radiol.2392042202. PMID:16569781.
- [75] Deng J, Miller FH, Rhee TK, et al. Diffusion-weighted MR imaging for determination of hepatocellular carcinoma response to yttrium-90 radioembolization. *J Vasc Interv Radiol* 2006; 17: 1195–1200. doi:10.1097/01.RVI.0000227234.81718.EB. PMID:16868174.
- [76] Dzik-Jurasz A, Domenig C, George M, et al. Diffusion MRI for prediction of response of rectal cancer to chemoradiation. *Lancet* 2002; 360: 307–308. doi:10.1016/S0140-6736(02)09520-X. PMID:12147376.
- [77] Do RK, Chandarana H, Felker E, et al. Diagnosis of liver fibrosis and cirrhosis with diffusion-weighted imaging: value of normalized apparent diffusion coefficient using the spleen as reference organ. *AJR Am J Roentgenol* 2010; 195: 671–676. doi:10.2214/AJR.09.3448. PMID:20729445.
- [78] Sandrasegaran K, Akisik FM, Lin C, et al. Value of diffusion-weighted MRI for assessing liver fibrosis and cirrhosis. *AJR Am J Roentgenol* 2009; 193: 1556–1560. doi:10.2214/AJR.09.2436. PMID:19933647.
- [79] Bulow R, Mensel B, Meffert P, Hernando D, Evert M, Kuhn JP. Diffusion-weighted magnetic resonance imaging for staging liver fibrosis is less reliable in the presence of fat and iron. *Eur Radiol* 2012; doi:10.1007/s00330-012-2700-2.
- [80] Tosun M, Inan N, Sarisoy HT, et al. Diagnostic performance of conventional diffusion weighted imaging and diffusion tensor imaging for the liver fibrosis and inflammation. *Eur J Radiol* 2013; 82: 203–207. doi:10.1016/j.ejrad.2012.09.009. PMID:23122674.
- [81] Kovac JD, Dakovic M, Stanisavljevic D, et al. Diffusion-weighted MRI versus transient elastography in quantification of liver fibrosis in patients with chronic cholestatic liver diseases. *Eur J Radiol* 2012; 81: 2500–2506. doi:10.1016/j.ejrad.2011.10.024. PMID:22100369.
- [82] Bakan AA, Inci E, Bakan S, Gokturk S, Cimilli T. Utility of diffusion-weighted imaging in the evaluation of liver fibrosis. *Eur Radiol* 2012; 22: 682–687. doi:10.1007/s00330-011-2295-z. PMID:21984447.
- [83] Bonekamp S, Torbenson MS, Kamel IR. Diffusion-weighted magnetic resonance imaging for the staging of liver fibrosis. *J Clin Gastroenterol* 2011; 45: 885–892. doi:10.1097/MCG.0b013e318223bd2c. PMID:21716125.
- [84] Soylu A, Kilickesmez O, Poturoglu S, et al. Utility of diffusion-weighted MRI for assessing liver fibrosis in patients with chronic active hepatitis. *Diagn Interv Radiol* 2010; 16: 204–208. PMID:20658448.
- [85] Mwangi I, Hanna RF, Kased N, et al. Apparent diffusion coefficient of fibrosis and regenerative nodules in the cirrhotic liver at MRI. *AJR Am J Roentgenol* 2010; 194: 1515–1522. doi:10.2214/AJR.09.3484. PMID:20489091.
- [86] Wang QB, Zhu H, Liu HL, Zhang B. Performance of magnetic resonance elastography and diffusion-weighted imaging for the staging of hepatic fibrosis: a meta-analysis. *Hepatology* 2012; 56: 239–247. doi:10.1002/hep.25610. PMID:22278368.
- [87] Watanabe H, Kanematsu M, Goshima S, et al. Staging hepatic fibrosis: comparison of gadoxetate disodium-enhanced and diffusion-weighted MR imaging—preliminary observations. *Radiology* 2011; 259: 142–150. doi:10.1148/radiol.10100621. PMID:21248234.
- [88] Yang DM, Jahng GH, Kim HC, et al. The detection and discrimination of malignant and benign focal hepatic lesions: T2 weighted vs diffusion-weighted MRI. *Br J Radiol* 2011; 84: 319–326. doi:10.1259/bjr/50130643. PMID:20959371.
- [89] Coenegrachts K, Matos C, ter Beek L, et al. Focal liver lesion detection and characterization: comparison of non-contrast enhanced and SPIO-enhanced diffusion-weighted single-shot spin echo planar and turbo spin echo T2-weighted imaging. *Eur J Radiol* 2009; 72: 432–439. doi:10.1016/j.ejrad.2008.09.005. PMID:18849130.
- [90] Bruegel M, Holzapfel K, Gaa J, et al. Characterization of focal liver lesions by ADC measurements using a respiratory triggered diffusion-weighted single-shot echo-planar MR imaging technique. *Eur Radiol* 2008; 18: 477–485. doi:10.1007/s00330-007-0785-9. PMID:17960390.
- [91] Goshima S, Kanematsu M, Kondo H, et al. Diffusion-weighted imaging of the liver: optimizing b value for the detection and characterization of benign and malignant hepatic lesions. *J Magn Reson Imaging* 2008; 28: 691–697. doi:10.1002/jmri.21467. PMID:18777553.
- [92] Coenegrachts K, Delanote J, Ter Beek L, et al. Improved focal liver lesion detection: comparison of single-shot diffusion-weighted echoplanar and single-shot T2 weighted turbo spin echo techniques. *Br J Radiol* 2007; 80: 524–531. doi:10.1259/bjr/33156643. PMID:17510250.
- [93] Ichikawa T, Haradome H, Hachiya J, Nitatori T, Araki T. Characterization of hepatic lesions by perfusion-weighted MR imaging with an echoplanar sequence. *AJR Am J Roentgenol* 1998; 170: 1029–1034. doi:10.2214/ajr.170.4.9530054. PMID:9530054.
- [94] Song KD, Kim YK, Lee WJ, et al. Detection and characterization of small focal hepatic lesions ( $\leq 2.5$  cm in diameter): a

- comparison of diffusion-weighted images before and after administration of gadoxetic acid disodium at 3.0T. *Acta Radiol* 2012; 53: 485–493. doi:10.1258/ar.2012.110437. PMID:22535883.
- [95] Kim YK, Lee MW, Lee WJ, et al. Diagnostic accuracy and sensitivity of diffusion-weighted and of gadoxetic acid-enhanced 3-T MR imaging alone or in combination in the detection of small liver metastasis ( $\leq 1.5$  cm in diameter). *Invest Radiol* 2012; 47: 159–166. PMID:22330426.
- [96] Chung WS, Kim MJ, Chung YE, et al. Comparison of gadoxetic acid-enhanced dynamic imaging and diffusion-weighted imaging for the preoperative evaluation of colorectal liver metastases. *J Magn Reson Imaging* 2011; 34: 345–353. doi:10.1002/jmri.22671. PMID:21702068.
- [97] Lowenthal D, Zeile M, Lim WY, et al. Detection and characterisation of focal liver lesions in colorectal carcinoma patients: comparison of diffusion-weighted and Gd-EOB-DTPA enhanced MR imaging. *Eur Radiol* 2011; 21: 832–840. doi:10.1007/s00330-010-1977-2. PMID:20886339.
- [98] Shimada K, Isoda H, Hirokawa Y, Arizono S, Shibata T, Togashi K. Comparison of gadolinium-EOB-DTPA-enhanced and diffusion-weighted liver MRI for detection of small hepatic metastases. *Eur Radiol* 2010; 20: 2690–2698. doi:10.1007/s00330-010-1842-3. PMID:20563726.
- [99] Nasu K, Kuroki Y, Kuroki S, Murakami K, Nawano S, Moriyama N. Diffusion-weighted single shot echo planar imaging of colorectal cancer using a sensitivity-encoding technique. *Jpn J Clin Oncol* 2004; 34: 620–626. doi:10.1093/jjco/hyh108. PMID:15591461.
- [100] Cieszanowski A, Szeszkowski W, Golebiowski M, Bielecki DK, Grodzicki M, Pruszyński B. Discrimination of benign from malignant hepatic lesions based on their T2-relaxation times calculated from moderately T2-weighted turbo SE sequence. *Eur Radiol* 2002; 12: 2273–2279. PMID:12195480.